8 March 2026

Fabrication of Sub-20 µm Microfluidic Channels Using Low-Cost FDM 3D-Printed Molds -A Lab-on-Cheap Approach

Wissal El Majdoub[1,2], Francesco Petrini[3], Ester Te Lindert -Blommert[4], Klaus Mathwig[2], Aldrik H Velders[1], Giovanni Valenti[3], Vittorio Saggiomo[1]

1. Wageningen University and Research
2. imec within OnePlanet Research Center
3. Department of Chemistry "Giacomo Ciamician" Alma Mater Studiorum -University of Bologna
4. Wageningen Electron Microscopy Centre Wageningen University and Research

Abstract

In surface-based biosensors, an optimal microchannel geometry combines a large surface area in the XY plane with a reduced channel height along the Z-axis. However, fabricating microchannels with heights below 25 µm and/or incorporating micropillars remains challenging using low-cost, accessible methods. Here, we propose a simple and rapid fabrication method that exploits the intrinsic surface topography generated by fused deposition modelling (FDM) 3D printing. This layer-by-layer fabrication process inherently produces surface features that were exploited to form microchannels. The substrates were characterized to determine the dimensions and geometries using scanning electron microscopy (SEM), fluorescence microscopy, confocal microscopy, and 3D reconstructions. The results showed that surface features from the 3D-printed molds were successfully transferred into polydimethylsiloxane (PDMS). When pressed to glass, the PDMS replicas form adjacent microchannels as small as 15 µm in height that provide a shallow and extensive sensing area. Flow tests confirmed the integrity of the channels and demonstrated that they could be sealed without plasma bonding. This approach demonstrates a significant advancement in the fabrication of sub-20 µm microchannels and in the development of alternatives to traditional micropillars, with high-resolution results achieved using standard, low-cost FDM printing.

 https://doi.org/10.26434/chemrxiv.15000686/v1

Keywords

microfluidics, 3d printing

Journal Name

ARTICLE TYPE

Fabrication of Sub-20 µm Microfluidic Channels Using Low-Cost FDM 3D-Printed Molds – A Lab-on-Cheap Approach†

Cite this: DOI: 00.0000/xxxxxxxxxx

Wissal El Majdoub,[a,b] Francesco Petrini,[c] Ester te Lindert - Blommert,[d] Klaus Mathwig, [b] Aldrik H. Velders, [a] Giovanni Valenti, [c] and Vittorio Saggiomo ,*[a]

Received Date
Accepted Date

DOI: 00.0000/xxxxxxxxxx

In surface-based biosensors, an optimal microchannel geometry combines a large surface area in the XY plane with a reduced channel height along the Z-axis. However, fabricating microchannels with heights below 25 µm and/or incorporating micropillars remains challenging using low-cost, accessible methods. Here, we propose a simple and rapid fabrication method that exploits the intrinsic surface topography generated by fused deposition modelling (FDM) 3D printing. This layer-by-layer fabrication process inherently produces surface features that were exploited to form microchannels. The substrates were characterized to determine the dimensions and geometries using scanning electron microscopy (SEM), fluorescence microscopy, confocal microscopy, and 3D reconstructions. The results showed that surface features from the 3D-printed molds were successfully transferred into polydimethylsiloxane (PDMS). When pressed to glass, the PDMS replicas form adjacent microchannels as small as 15 µm in height that provide a shallow and extensive sensing area. Flow tests confirmed the integrity of the channels and demonstrated that they could be sealed without plasma bonding. This approach demonstrates a significant advancement in the fabrication of sub-20 µm microchannels and in the development of alternatives to traditional micropillars, with high-resolution results achieved using standard, low-cost FDM printing.

1 Introduction

Microfluidics has gained growing interest in biomedical applications [1–3] and is widely used in areas such as cell processing, [4–7] drug discovery, [8–11] pharmacological and toxicological assays, [8,12,13] tissue engineering, [14] and organ-on-chip platforms. [6,15,16]

Microfluidics is also central in the integration of biosensors into lab-on-chip systems. [17–20] These systems enable precise handling of small fluid volumes, reducing reagent consumption, accelerating biochemical reactions, and enhancing detection sensitivity. The complete sample analysis can be integrated onto a single portable platform with high throughput and reduced operational costs while using minimal reagent volumes, making it suitable for point-of-care applications. [18]

Microchannels are key structures in microfluidics, and their dimensions must be carefully considered. [21] In surface-based biosensors, reducing the microchannel height drastically increases the diffusion rate of analytes to the sensor surface. This enhancement in mass transport fastens the analyte interactions and thereby shortens the sensor's response time and increases its sensitivity. [22–24] Another important design consideration for microchannels in surface-based biosensors is their lateral dimensions. While a small channel height enhances analyte diffusion toward the active surface, wide and elongated channels can provide an extended active surface, thereby increasing the probability of analyte binding.

In addition to the microchannel dimensions, one must also consider their fabrication method and the choice of material. Polydimethylsiloxane (PDMS) is the most widely used material for that matter. [25,26] PDMS shows many advantages: it is low-cost, biocompatible, transparent, and easy to handle. Its surface can be modified using silane chemistry, and it has a high gas permeability, which supports the viability of cells and microorganisms. Typically, PDMS microchannels are fabricated by replicating a silicon master mold produced through clean-room lithography, [27,28]

[a] *BioNanoTechnology, Wageningen University and Research, Bornse Weilanden 9, 6708 WG Wageningen, the Netherlands.*
[b] *imec within OnePlanet Research Center, Bronland 10, 6708 WH Wageningen, the Netherlands.*
[c] *Department of Chemistry "Giacomo Ciamician", Alma Mater Studiorum – University of Bologna, Via Gobetti 85, 40129 Bologna, Italy.*
[d] *Wageningen Electron Microscopy Centre, Wageningen University and Research, Droevendaalsesteeg 1, 6708 PB Wageningen, the Netherlands.*

† Additional footnotes to the title and authors can be included *e.g.* 'Present address:' or 'These authors contributed equally to this work' as above using the symbols: ‡, §, and ¶. Please place the appropriate symbol next to the author's name and include a `\footnotetext` entry in the the correct place in the list.

or stereolithography (SLA) 3D printing.[29–31] After casting and curing the PDMS on the mold, it is peeled off and bonded to a glass substrate via oxygen plasma activation.

To fabricate PDMS microchannels with large lateral dimensions and small heights, supporting micropillars are often integrated to prevent the collapse of the PDMS "roof".[32] These pillars are also usually fabricated by replicating silicon master molds made in clean rooms.[33,34] While this approach achieves excellent feature resolution (with heights below 5 μm), it requires clean-room processes, which are costly, complex, and time-consuming.

3D printing has been reported as a versatile alternative for the fabrication of microfluidic devices.[35–41] Compared to conventional cleanroom lithography, 3D printing enables rapid and low-cost prototyping. Among the various additive manufacturing techniques, SLA and fused deposition modeling (FDM) 3D printing are the most accessible commercial approaches. These techniques can be used either to directly print microfluidic devices or to fabricate molds for subsequent PDMS replication.[29–31,42]

SLA printing uses photopolymerization to achieve fine feature resolution and smooth surfaces. However, it faces challenges when fabricating features below 25 μm in the Z direction, and 50 μm in the XY plane, as controlling light exposure and polymerization at small scales becomes more difficult.[43,44] These limitations often lead to partial resin curing. When SLA printing is used to directly fabricate microfluidic devices, uncured resin can remain trapped within enclosed microchannels and is difficult to remove. In the case of PDMS replication, partial resin curing can lead to incomplete PDMS crosslinking due to residual monomers or photoinitiators, resulting in fragile demolding.[44] Although insightful work has investigated the fabrication of features below 100 μm using SLA printing, the processes remain complex and non-intuitive.[29,45–48] SLA has also been used to fabricate micropillars, but the smallest pillar structures have dimensions of 50 μm $\times$ 50 μm $\times$ 100 μm, which remain limited and impractical.[46] Therefore, there is a need to develop easier methods to fabricate microchannels with small heights and large lateral dimensions to advance microfluidic device prototyping.

FDM printing is generally cheaper than SLA printing, and its fabrication principle is simpler. A thermoplastic filament is extruded through a heated nozzle and deposited layer by layer to form the desired 3D structure. The printing resolution in the XY plane depends on several interdependent parameters, including the nozzle diameter, the extrusion temperature, and the nozzle-to-build-plate distance. The precise control of these parameters is challenging and limits the resolution of FDM-printed structures in the XY plane to 200 μm with standard 0.4 mm nozzles.[49] The Z-axis resolution in FDM 3D printing corresponds to the thickness of each layer of filament deposited and is easy to control. However, the layer-by-layer fabrication principle inherently introduces a periodic ridge-and-valley structure along the Z-axis that creates porosity in the printed object, reducing its ability to contain pressurized fluids. Furthermore, this porosity leads to reduced optical quality in PDMS replicas and hinder reliable sealing or bonding of the replicas to glass substrates.[49,50] As a result, FDM printing is typically used to fabricate microfluidic devices with larger channel sizes rather than molds for subsequent PDMS replication.

Here, we exploit this layering limitation and we treat the Z-axis resolution of FDM 3D printing as a strength rather than a limitation. We show that the ridge-and-valley structures along the Z-axis can be replicated in PDMS to form microchannels with small heights by sticking the PDMS to a glass surface. Moreover, because the so formed microchannels are adjacent to one another, they collectively provide a large surface area. The present study therefore introduces a low-cost, accessible, and rapid alternative to traditional micropillars. Here, we explore the use of standard FDM 3D printing for microchannels fabrication, and we evaluate the fidelity and dimensional accuracy of the resulting structures. The workflow is accessible even to non-experts and is suitable for diverse biomedical applications, such as surface-based biosensing (e.g. electrochemical biosensing).

2 Results and discussion

We exploit the intrinsic surface features of FDM 3D-printed structures to form PDMS microchannels. The layer-by-layer fabrication process of FDM 3D printing generates ridges and valleys along the Z-axis, which we replicate negatively in PDMS and assemble onto a glass substrate to form microchannels.

For this purpose, we printed a flat structure made of polylactic acid (PLA) in the vertical orientation to maximize the presence of the surface patterns along the Z-axis, which would be largely diminished if the structure was printed horizontally (Figure 1a). The PDMS mixture was cast directly onto the printed structure, which was fixed horizontally (Figure 1b,c). The PDMS was cured and carefully peeled off from the printed mold (Figure 1d).

The PLA mold with the maximum printing layer resolution of 50 μm and its corresponding PDMS replica were characterized using scanning electron microscopy (SEM) to identify their dimensions and surface morphology. SEM of the PLA mold (Figure 2a) confirms the presence of ridge-and-valley structures with an average valley depth of around 15 μm. SEM analysis of the PDMS replica (Figure 2b) confirms uniform replication of the curved geometry and an average half-pipe depth also of around 15 μm. A full 3D reconstruction of the SEM data, allowing detailed observation of both substrate surfaces, is provided in the supplementary information (Figure S1, S2).

The PDMS replicas from molds of varying layer thicknesses (namely 50, 100, 150 and 200 μm) were dyed with rhodamine and observed by fluorescence microscopy. The microscopic image of their cross-section (Figure 3) clearly highlights the resulting structures corresponding to half-pipes. The microscopic images in the bright-field mode are also shown in the supplementary information (Figure S3). The results show that the Z-axis resolution (layer thickness) of the printed structure directly determines the final height of the half-pipe structures formed in PDMS.

We confirm the reproducibility of the replication by using a different FDM 3D printer, as detailed in the supplementary information (Figure S4).

The PDMS replica, with two holes for the inlet and outlet, was mechanically pressed onto the substrate to form the microchannels, which eliminates the need for plasma bonding. To achieve this, custom holders composed of four 3D-printed polyethylene terephthalate glycol (PETG) units were fabricated and assem-

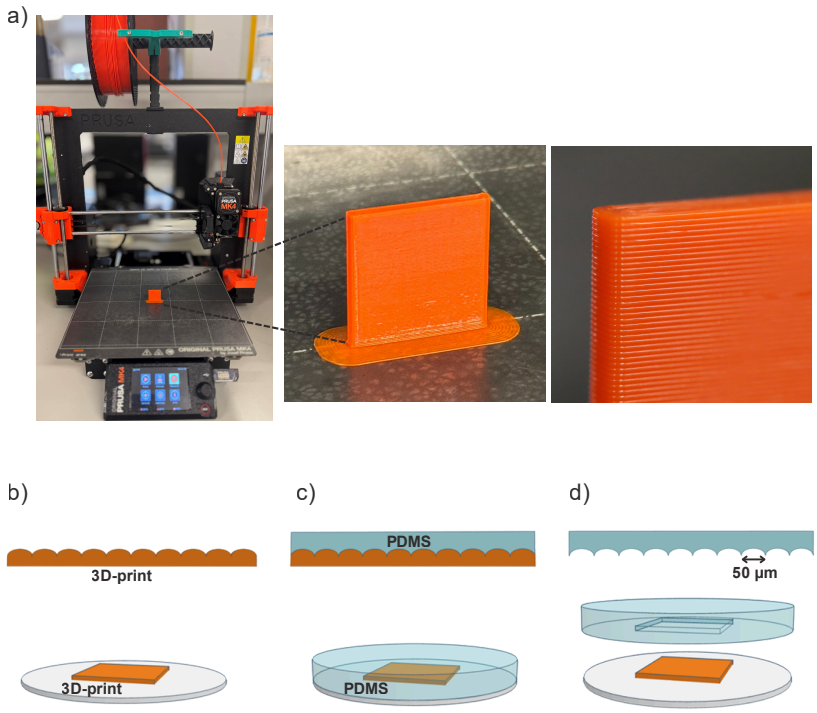

Fig. 1 a) The PLA mold (2cm×2cm×2mm) is printed vertically with an FDM 3D printer. The macropicture shows the layered structure. b) The printed mold (only the top is shown here) is fixed horizontally in a Petri dish. c) PDMS is cast directly on the printed mold. d) PDMS is carefully peeled off from the printed mold. The PDMS exposes the negative replication of the surface features of the printed PLA mold.

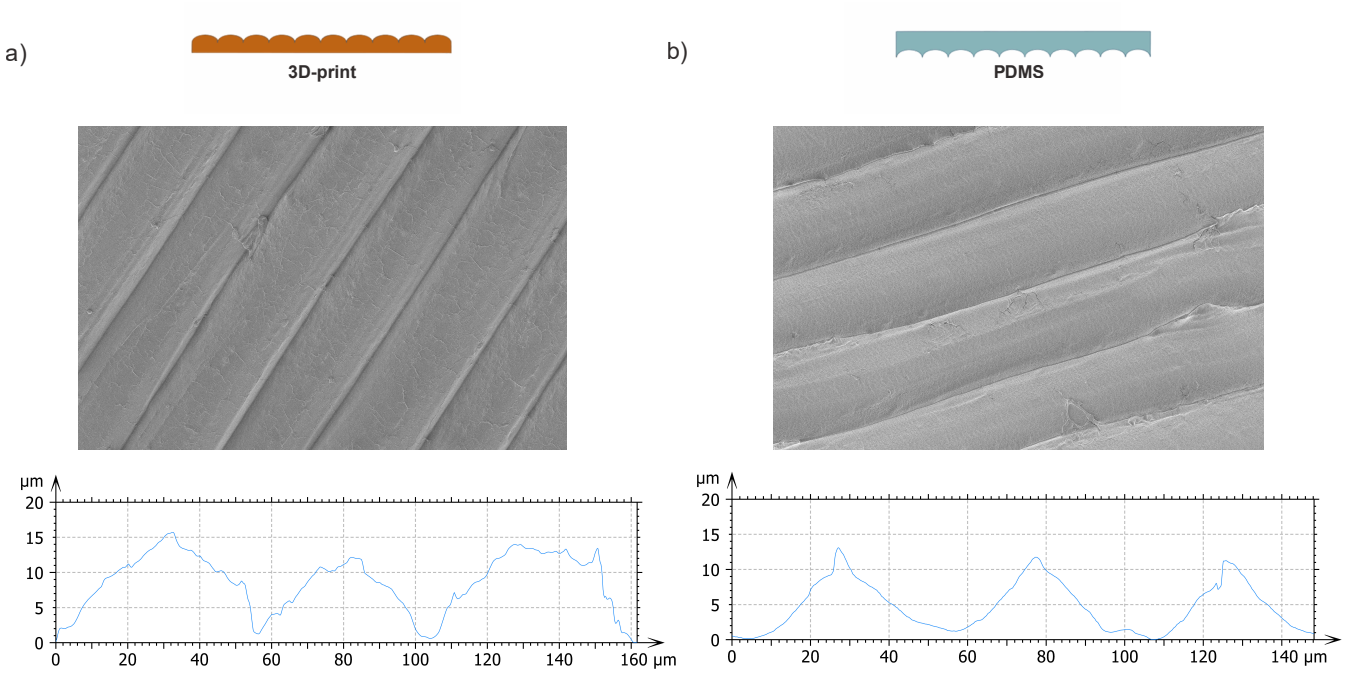

Fig. 2 SEM images (at +7°) and cross-sectional analysis of a) the PLA printed mold with 50 µm layer thickness b) the corresponding PDMS replica.

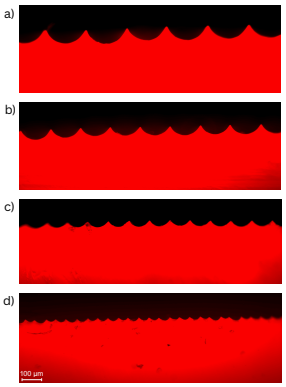

Fig. 3 10× fluorescence microscopy images of the cross-section of rhodamine-dyed PDMS replicas fabricated from printed molds with varying layer thicknesses: a) 200 µm, b) 150 µm, c) 100 µm, and d) 50 µm.

bled in pairs using screws (Figure 4). These holders allow PDMS chips with varying thickness to be pressed between a polymethyl methacrylate (PMMA) piece and a glass slide. The screws are tightened until the holders hardly move and remain still. Multiple microchannels are formed in parallel on the glass surface. Each microchannel has a volume of approximately 15 nL, assuming a rectangular cross-section and a channel length of 2 cm (which can be adjusted by varying the distance between the inlet and outlet apertures). When the inlet aperture reaches a diameter of 1.5 mm, a total of 30 parallel microchannels can be filled, resulting in a combined flow volume of approximately 0.5 μL.

To verify that the microchannels were properly sealed, a simple flow test with a solution of polystyrene (PS) beads was performed after fabrication. The PDMS chips were first inspected by eye to identify any immediate leakage or obvious sealing defects. The channels integrity and continuity were then verified by optical microscopy (Figure 5a).

To obtain a detailed observation of the channels' cross-section when filled with solution, confocal imaging was performed. An aqueous fluorescein solution was introduced into rhodamine-dyed PDMS microchannels. Imaging was carried out using both the rhodamine and fluorescein channels of the confocal microscope, enabling a clear distinction between the internal structure of the PDMS channels (fluorescein signal) and the PDMS material (rhodamine signal). By acquiring a z-stack of images, we obtained a qualitative 3D visualization that reveals the morphology of the filled channels (Figure 5b). The measured channel height of approximately 30 μm is not reliable. This inaccuracy is likely due to several parameters, such as a too large confocal spot size with the objective used, a potential bleaching of the fluorescein dye, a possible diffusion of the dye into the PDMS, or errors during data transfer from the confocal software to ImageJ.

To prove the integrity of the single channels, flow experiments using suspensions of polystyrene (PS) beads with a diameter of 1 μm in water were performed. Rhodamine-labelled PS beads were introduced at high-speed compared to the exposure time of the microscope and their trajectories appearing as continuous lines could be visualized by fluorescence microscopy (Figure 5c). The beads appear to remain confined within distinct microchannels; and slow down (dots) near the channel walls. A microscope video in the supplementary information shows that the beads flow without any crossflow between the channels. When PS beads with a diameter of 7 μm were introduced, they easily clogged the small channels (Figure 5d).

Our results show that PLA molds produced by FDM printing have well-defined ridge–and-valley structures on the surface with valley depths down to 15 μm. These patterns are successfully transferred into PDMS, as confirmed by fluorescence microscopy, SEM imaging, and confocal microscopy. Flow tests demonstrate that the replicated structures function as confined microchannels on a glass substrate even without plasma treatment.

Rather than designing micropillars, this approach uses the surface topography created by FDM printing to form multiple small, parallel microchannels. This avoids cleanroom fabrication, making the process faster and easier while achieving resolutions beyond those achievable with standard FDM 3D printing on the XY plane. This method also avoids the need for plasma equipment by using custom 3D-printed holders. Overall, the method is simple and low-cost. It can be replicated even with a low-quality FDM 3D printer, since the distance between the inlet and outlet apertures can be adjusted to have well-defined layers replicated in PDMS. Further miniaturization by optimizing printing parameters, such as extrusion multipliers, nozzle temperature, and printing speed, could be explored in future work.

3 Materials and methods

3.1 PDMS replication of 3D-printed mold

The PLA master mold (2 cm × 2 cm × 2 mm) was fabricated with a Prusa MK4 3D printer (Prusa Research, Prague, Czech Republic) equipped with a 0.4 mm nozzle. The PLA filament was purchased from REAL-filament (Amsterdam, the Netherlands). Model slicing and layer thickness were defined in the PrusaSlicer v2.9.0 software. SYLGARD™ 184 silicone elastomer base and curing agent (Dow Corning Corporation, Midland, MI, USA) were mixed with a 10:1 weight ratio, stirred manually for 3 min to ensure homogeneity, and subsequently degassed in a vacuum desiccator. The degassed PDMS mixture was then cast directly onto the PLA master mold (which was fixed with double sided-tape horizontally in a Petri-dish). The PDMS was left to cure at room temperature overnight to minimize air bubble formation. Final curing was performed in the oven at 70 °C for 2 h. After curing, the solidified PDMS, containing the negative replication of the 3D print surface features, was carefully peeled off the mold.

3.2 Scanning electron microscopy

We performed SEM (Magellan 400, FEI, Eindhoven, the Netherlands) to validate the surface reconstruction of the PLA master mold and the PDMS replica. Images were captured with the secondary electron detector set at 2 kV and 13 pA. Images were taken at +7° and -7°, allowing for the generation of 3D stereoscopic images. The images were obtained at 1000x magnification.

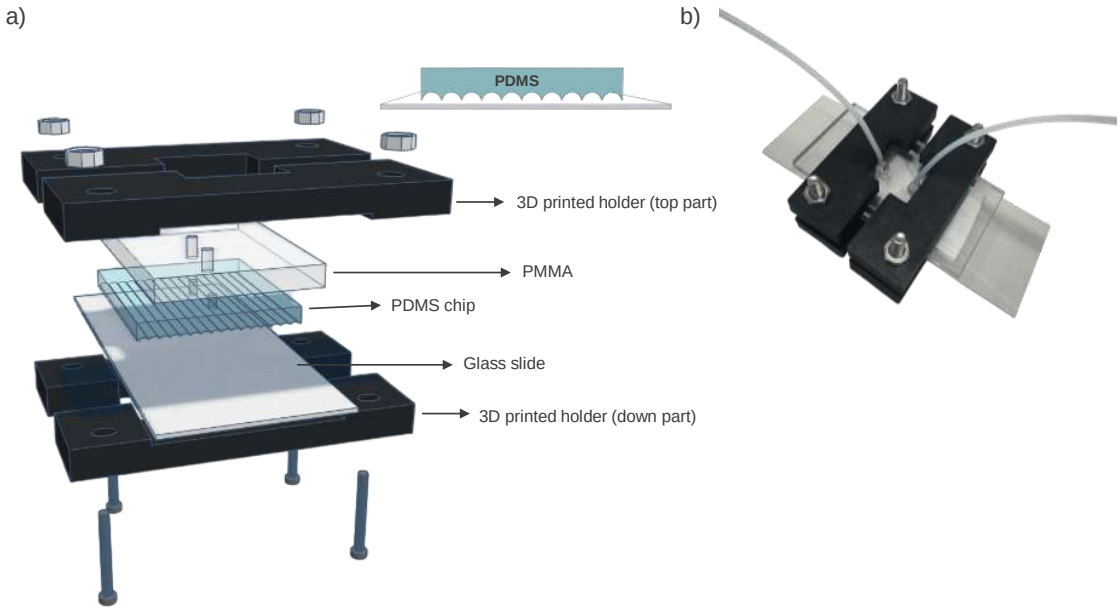

Fig. 4 a) Exploded view of the microfluidic device with 3D-printed holders pressing the PDMS chip to a glass slide b) Picture of the microfluidic device.

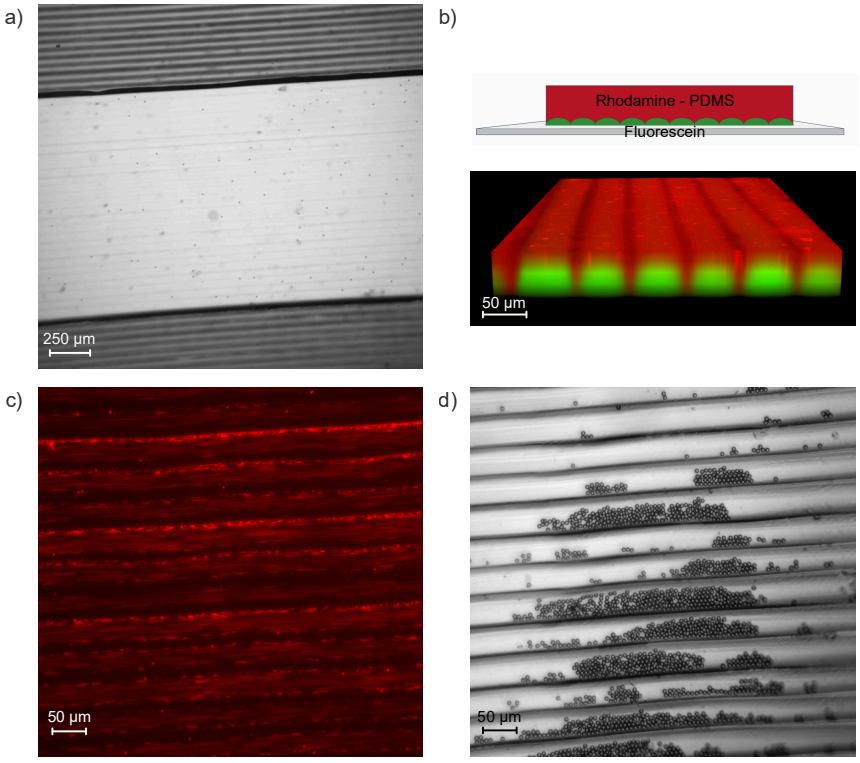

Fig. 5 a) 2.5× bright-field microscopy image showing the filling of the channels connected to the inlet with a PS bead suspension. Only the channels in the center are being filled, they remain sealed from the channels in the top and bottom of the image. b) 3D visualization of the microchannels' cross-section obtained from a confocal microscopy z-stack. The PDMS was dyed with rhodamine, and a fluorescein solution was introduced. c) 20× fluorescence microscopy image of 1 µm rhodamine-labeled PS beads introduced into the channel at a flow rate of 0.1 mL/min. d) 20× fluorescence microscopy image of 7 µm PS beads introduced at a flow rate of 10 µL/min.

3.3 Analysis in MountainsSEM®

Stereoscopic 3D reconstruction of the PLA master and the PDMS replica was performed using MountainsSEM® software (Digital Surf, Besançon, France). For 3D reconstruction, a comparison window of 5x5 pixels was used. During post-processing, images were leveled. With the 3D reconstruction, a profile curve was made to extract the height profile of the samples.

3.4 PDMS-on-glass microchannels

The PDMS replica was attached to a microscope glass slide to enclose the microchannels using a custom 3D-printed clamping system. Before assembly, both the PDMS substrate and the glass slide were thoroughly cleaned with isopropanol and Milli-Q water, then dried. Remaining dust particles were removed using adhesive tape. Inlet and outlet holes were created through the PDMS using a 1.5 mm biopsy punch. The clamping system was designed using the open-access online software *Tinkercad* (Autodesk, San Francisco, CA, USA). It was fabricated from PETG (Prusa Research), a material chosen for its greater mechanical stability compared to PLA. It was used to press the PDMS replica between a PMMA piece and a glass substrate. The clamp was positioned immediately before the inlet and immediately after the outlet to prevent liquid from flowing outside of the channel region.

3.5 Fluorescence microscopy

The PDMS replica was cut with a scalpel to expose the cross-section, which was then visualized using a Leica DMi8 microscope (Leica Microsystems, Wetzlar, Germany) in bright-field mode and rhodamine mode. To enhance contrast, the PDMS samples were immersed in a dichloromethane (DCM) solution containing Rhodamine B (Sigma-Aldrich, St. Louis, MO, USA) for several minutes and then dried. Swelling of the PDMS in DCM facilitates diffusion of the dye through the PDMS, giving it a light red coloration. This helped to properly visualize the cross-section of the PDMS replica in the Rhodamine channel of the microscope. To evaluate reproducibility, identical experiments were conducted with PDMS replicas fabricated from molds printed using a Bambu Lab A1 3D printer (Shenzhen, China).

3.6 Flow trials

PS beads with diameters of 1 μm and 7 μm (Sigma-Aldrich) were suspended in Milli-Q water and introduced into the channels using a syringe connected to a Pump 11 Elite pump (Harvard Apparatus, Holliston, MA, USA). Flow was introduced in withdrawing mode to prevent detachment of the channels from the glass substrate. 1 μm rhodamine-PS beads were introduced at a higher flow rate (0.1 mL/min corresponding to a speed of 75 mm/s) than the exposure time of the microscope (90 s) to observe their trajectory; and 7 μm PS beads were introduced at 10 μL/min (corresponding to a speed of 7.5 mm/s).

3.7 Confocal microscopy

Fluorescein free acid was purchased from Sigma-Aldrich, and fluorescein solutions were prepared in Milli-Q water and stabilized with sodium hydroxide. Confocal fluorescence imaging was performed using an RCM confocal microscope (Confocal.NL, Amsterdam, the Netherlands) to visualize the interior of the microchannels filled with fluid. Imaging was performed with a 20x objective at a Z-step of 5 μm. The acquired image stacks were processed using the open-source software Fiji (National Institutes of Health, Bethesda, MD, USA) to generate a 3D visualization. It enabled the confirmation of the channels' cross-section geometry under flow conditions. This experiment was conducted in rhodamine-dyed PDMS microchannels to provide a clear contrast between the interior and exterior of the channels.

Conclusions

In this work, we introduce a simple and cost-friendly way of fabricating 15 μm PDMS microchannels. We used 3D FDM printers, which are easy to use, and ubiquitous nowadays to perform replica molding. The FDM printer can be used to fabricate microchannels of various sizes by tuning the thickness of the printed layers. The volume can be modified by changing the length of the microchannels (distance between the inlet and outlet apertures) and the inlet and outlet apertures' sizes.

Through this technology, we developed an open way to fabricate microdevices for researchers or students less experienced in microfabrication. The continuous advancement of 3D printing technologies and the growing interest in their applications suggest that higher Z-axis resolution will become available in the future, enabling the fabrication of even smaller microchannels. These systems can be used for simple fluid handling and for more advanced applications for instance in surface-based biosensing.

Author contributions

Wissal El Majdoub [a,b]: Investigation, Methodology, Validation, Data curation, Visualization, Original draft writing, Review and editing

Francesco Petrini [c]: Investigation, Methodology, Validation, Review and editing

Esther te Lindert-Bloomert [d]: Methodology (SEM reconstructions), Review and editing

Klaus Mathwig [b]: Funding acquisition, Project administration , Supervision, Review and editing

Aldrik H. Velders [a]: Resources, Project administration , Supervision, Review and editing

Giovanni Valenti [c] : Funding acquisition, Supervision, Review and editing

Vittorio Saggiomo* a: Funding acquisition, Resources, Conceptualization, Investigation, Methodology, Data curation, Project administration , Supervision, Original draft writing, Review and editing

Conflicts of interest

There are no conflicts to declare.

Acknowledgements

The ECLectic project has received funding from the European Union's MSCA Doctoral network Horizon Europe program Grant Agreement Number 101119951. SEM analysis was conducted at the Wageningen Electron Microscopy Centre (WEMC) of Wageningen University and Research (WUR).

Notes and references

1 D. J. Beebe, G. A. Mensing and G. M. Walker, *Annual Review of Biomedical Engineering*, 2002, **4**, 261–286.

2 E. K. Sackmann, A. L. Fulton and D. J. Beebe, *Nature*, 2014, **507**, 181–189.

3 S. K. Sia and G. M. Whitesides, *Electrophoresis*, 2003, **24**, 3563–3576.

4 A. Benavente-Babace, D. Gallego-Pérez, D. Hansford, S. Arana, E. Pérez-Lorenzo and M. Mujika, *Biosensors and Bioelectronics*, 2014, **61**, 298–305.

5 S. Nagrath, L. V. Sequist, S. Maheswaran, D. W. Bell, D. Irimia, L. Ulkus, M. R. Smith, E. L. Kwak, S. Digumarthy, A. Muzikansky, P. Ryan, U. J. Balis, R. G. Tompkins, D. A. Haber and M. Toner, *Nature*, 2007, **450**, 1235–1239.

6 A. Rival, D. Jary, C. Delattre, Y. Fouillet, G. Castellan, A. Bellemin-Comte and X. Gidrol, *Lab on a Chip*, 2014, **14**, 3739–3749.

7 W.-M. Zhou, Y.-Y. Yan, Q.-R. Guo, H. Ji, H. Wang, T.-T. Xu, B. Makabel, C. Pilarsky, G. He, X.-Y. Yu and J.-Y. Zhang, *Journal of Nanobiotechnology*, 2021, **19**, 312.

8 G. Caruso, N. Musso, M. Grasso, A. Costantino, G. Lazzarino, F. Tascedda, M. Gulisano, S. M. Lunte and F. Caraci, *Micromachines*, 2020, **11**, 593.

9 P. S. Dittrich and A. Manz, *Nature Reviews Drug Discovery*, 2006, **5**, 210–218.

10 A. Polini, L. Prodanov, N. S. Bhise, V. Manoharan, M. R. Dokmeci and A. Khademhosseini, *Expert Opinion on Drug Discovery*, 2014, **9**, 335–352.

11 P. Neužil, S. Giselbrecht, K. Länge, T. J. Huang and A. Manz, *Nature Reviews Drug Discovery*, 2012, **11**, 620–632.

12 M. D. Poskus, T. Wang, Y. Deng, S. Borcherding, J. Atkinson and I. K. Zervantonakis, *Microsystems Nanoengineering*, 2023, **9**, 140.

13 E. Novik, T. J. Maguire, P. Chao, K. Cheng and M. L. Yarmush, *Biochemical Pharmacology*, 2009, **79**, 1036–1044.

14 N. W. Choi, M. Cabodi, B. Held, J. P. Gleghorn, L. J. Bonassar and A. D. Stroock, *Nature Materials*, 2007, **6**, 908–915.

15 R. J. Abbed, E. I. Q. Cruz and S. E. Leggett, *bioRxiv*, 2025.

16 S. N. Bhatia and D. E. Ingber, *Nature Biotechnology*, 2014, **32**, 760–772.

17 J. P. Lafleur, A. Jönsson, S. Senkbeil and J. P. Kutter, *Biosensors and Bioelectronics*, 2015, **76**, 213–233.

18 G. Luka, A. Ahmadi, H. Najjaran, E. Alocilja, M. DeRosa, K. Wolthers, A. Malki, H. Aziz, A. Althani and M. Hoorfar, *Sensors*, 2015, **15**, 30011–30031.

19 L. Zhang, Q. Cai, R. S. Wiederkehr, M. Fauvart, P. Fiorini, B. Majeed, M. Tsukuda, T. Matsuno and T. Stakenborg, *Lab on a Chip*, 2016, **16**, 4012–4019.

20 Y.-L. Fang, C.-H. Wang, Y.-S. Chen, C.-C. Chien, F.-C. Kuo, H.-L. You, M. S. Lee and G.-B. Lee, *Lab on a Chip*, 2020, **21**, 113–121.

21 G. M. Whitesides, *Nature*, 2006, **442**, 368–373.

22 T. M. Squires, R. J. Messinger and S. R. Manalis, *Nature Biotechnology*, 2008, **26**, 417–426.

23 K. Awawdeh, M. A. Buttkewitz, J. Bahnemann and E. Segal, *Microsystems Nanoengineering*, 2024, **10**, 100.

24 S. Kang and J. J. Davis, *Chemical Science*, 2025, **16**, 6965–6974.

25 J. C. McDonald and G. M. Whitesides, *Accounts of Chemical Research*, 2002, **35**, 491–499.

26 N. Convery and N. Gadegaard, *Micro and Nano Engineering*, 2019, **2**, 76–91.

27 D. C. Duffy, J. C. McDonald, O. J. A. Schueller and G. M. Whitesides, *Analytical Chemistry*, 1998, **70**, 4974–4984.

28 Y. Xia, J. J. McClelland, R. Gupta, D. Qin, X. Zhao, L. L. Sohn, R. J. Celotta and G. M. Whitesides, *Advanced Materials*, 1997, **9**, 147–149.

29 S. B. J. Willems, J. Zegers, A. Bunschoten, R. M. Wagterveld, F. W. B. Van Leeuwen, A. H. Velders and V. Saggiomo, *The Analyst*, 2020, **145**, 1629–1635.

30 A. M. Garcia, J. A. Garcia-Romero, S. H. Mejias, P. Prieto, V. Saggiomo, A. H. Velders, M. L. Soriano, V. Ruiz-Díez, J. Cabanillas-González and M. V. Gomez, *Journal of Materials Chemistry C*, 2024, **12**, 6027–6034.

31 S. O. Woo, M. Oh and Y. Choi, *STAR Protocols*, 2022, **3**, 101376.

32 Y.-R. K.-B. Lee, Jin-Yong;Yun Young-Keu;Kim, *Bulletin of the Korean Chemical Society*, 2009, **30**, 1793–1797.

33 K. N. Hass, M. Bao, Q. He, L. Liu, J. He, M. Park, P. Qin and K. Du, *ACS Omega*, 2020, **5**, 27433–27441.

34 K. Chen and Z. Wang, *Methods and Protocols*, 2023, **6**, 80.

35 S. Waheed, J. M. Cabot, N. P. Macdonald, T. Lewis, R. M. Guijt, B. Paull and M. C. Breadmore, *Lab on a Chip*, 2016, **16**, 1993–2013.

36 C. M. B. Ho, S. H. Ng, K. H. H. Li and Y.-J. Yoon, *Lab on a Chip*, 2015, **15**, 3627–3637.

37 J. M. Lee, M. Zhang and W. Y. Yeong, *Microfluidics and Nanofluidics*, 2016, **20**, year.

38 K.-I. Kamei, Y. Mashimo, Y. Koyama, C. Fockenberg, M. Nakashima, M. Nakajima, J. Li and Y. Chen, *Biomedical Microdevices*, 2015, **17**, 36.

39 C. I. Rogers, K. Qaderi, A. T. Woolley and G. P. Nordin, *Biomicrofluidics*, 2015, **9**, 016501.

40 J.-Y. Lee, J. An and C. K. Chua, *Applied Materials Today*, 2017, **7**, 120–133.

41 L. Zhou, J. Fu and Y. He, *Advanced Functional Materials*, 2020, **30**, year.

42 J. C. McDonald, M. L. Chabinyc, S. J. Metallo, J. R. Anderson, A. D. Stroock and G. M. Whitesides, *Analytical Chemistry*, 2002, **74**, 1537–1545.

43 B. Venzac, S. Deng, Z. Mahmoud, A. Lenferink, A. Costa,

F. Bray, C. Otto, C. Rolando and S. L. Gac, *Analytical Chemistry*, 2021, **93**, 7180–7187.
44 B. Venzac, *Lab on a Chip*, 2025, **25**, 2129–2147.
45 H. Gong, B. P. Bickham, A. T. Woolley and G. P. Nordin, *Lab on a Chip*, 2017, **17**, 2899–2909.
46 A. Vedhanayagam, M. Golfetto, J. L. Ram and A. S. Basu, *Micromachines*, 2023, **14**, 1519.
47 P. J. E. M. Van Der Linden, A. M. Popov and D. Pontoni, *Lab on a Chip*, 2020, **20**, 4128–4140.
48 A. H. Velders, L. Van Lieshout, E. A. T. Brienen, B. Diederich and V. Saggiomo, *chemrxiv*, 2023.
49 N. Zhang, Z. Wang, Z. Zhao, D. Zhang, J. Feng, L. Yu, Z. Lin, Q. Guo, J. Huang, J. Mao and J. Yang, *Microsystems Nanoengineering*, 2025, **11**, 35.
50 A. V. Nielsen, M. J. Beauchamp, G. P. Nordin and A. T. Woolley, *Annual Review of Analytical Chemistry*, 2019, **13**, 45–65.